Effect of Zn and Mn Substitution on Structural, Dielectric, Magnetic and Optical Properties of Multiferroic $CoFe_2O_4$-$BaTiO_3$ Core-Shell Type Composites

Sourav Sarkar, J. Shah, R. K. Kotnala, M. C. Bhatnagar

Abstract: ***In this paper, we have reported the synthesis of Zn and Mn substituted cobalt ferrite by chemical co-precipitation method and used it as core material in barium titanate sol to finally prepare core-shell type composite material. Amount of ferrite was varied in the final composite samples from 30% to 50%. X-ray diffraction show prominent spinel and perovskite peaks corresponding to ferrite and titanate phases respectively. HRTEM micrographs reveal core-shell type nature with presence of a well-defined interface. Our proposed substitutions increase the resistivity of pure cobalt ferrite by one order which has been verified through I-V measurement. SEM micrographs show dense microstructure and particle formation of both phases in the composites. Substitution of Zn at the site of Co is supported by the peak shift in Attenuated Total Reflection Fourier Transform Infrared (ATR-FTIR) spectroscopy. Maxwell Wagner relaxation phenomena at the interface and hopping conduction in ferrites explain both frequency and temperature variation of dielectric parameters. Substitution of Zn and Mn result in super-paramagnetic type behavior with coercively ~ few Oe and very negligible remnant magnetization (M_R). Photoluminescence (PL) spectra show slight decrease in energy band gap of ferrite as a result of these substitutions.***

Keywords: Sol-gel process (A); Composites (B); Dielectric properties (C); Optical properties (C)

I. INTRODUCTION

Advancement in the work on multiferroics has taken a flurry in last decade though studies in these type of materials started as far back as in 1970's [1–4]. The extraordinary feature of these materials that they are magnetically polarizable as well as electrically magnetizable [5,6] has been intriguing researchers worldwide from quite some time. To realize both properties in a single material is a tricky job though as they require different kind of electronic configurations. While ferromagnetism requires unpaired electrons which interact through exchange bias mechanism, transition metal ions should have an empty 3d orbital to realize ferroelectricity [7,8]. This basic contrast is the main reason behind the deficiency of single phase multiferroic materials. Among them, Two most well-known materials are $BiFeO_3$ and Cr_2O_3. Despite being extensively studied, they do not deem suitable for practical applications. Firstly, they offer very less magnetoelectric coupling, making it difficult to use them for device design purpose. Also their low Curie temperature restricts their use only near room temperature. Composite multiferroics come to our rescue with feasible solutions to these problems.

The mere presence of two ferroic phases (i.e. ferroelectric, ferromagnetic or ferroelastic) in a composite is not sufficient for a good multiferroic material. Strong coupling interaction between them is the most essential requirement. The most common mechanism to realize multiferroic effect in a composite is mechanical strain-stress response at the interface of the two phases. Since most ferromagnetic materials show good magnetostrictive property, certain strain develops in them when they are subjected to magnetic field. This strain propagates to the ferroelectric phase via interface and causes stress. Due to piezoelectric property of ferroelectric materials, this stress generates electric potential, thus giving rise to magnetoelectric effect [6]. Mathematically magnetoelectric voltage coefficient for (α_E) is defined by the equation,

$\alpha_E = dE/dH = V/(d.H)$ where V is the measured induced voltage, d is the effective thickness of the piezoelectric phase and H is the amplitude of the applied magnetic field [5]

Now different structures of these composites like particulate composites, multilayer composites, thin film structures etc. offer different values of α_E. Among them, core shell like structure have some advantages over others, such as presence of prominent interface, relatively easier poling capability etc. [9,10].Here we have substituted Mn at the site of Fe and Zn at the site of Co in $CoFe_2O_4$ in optimized proportion so that the resistivity becomes higher than pure $CoFe_2O_4$. It is essential for better poling purpose. So our system under study is (x) $Co_{0.6}Zn_{0.4}Fe_{1.7}Mn_{0.3}O_4$- (1-x) $BaTiO_3$ (CZFMO-BTO) where ferromagnetic CZFMO is the core, ferroelectric BTO is the surrounding shell and x=0.3, 0.4, 0.5. In this paper we try to elaborate the changes that these substitutions bring in structural, dielectric, magnetic and optical properties of $CoFe_2O_4$-$BaTiO_3$ (CFO-BTO) core shell like composites.

II. EXPERIMENTAL DETAILS

$Co(NO_3)_2$, $Zn(NO_3)_2$, $Fe(NO_3)_3$and $Mn(NO_3)_2$ were the starting reagents in preparation of CFO and CZFMO nanoparticles by

Revised Version Manuscript Received on September 30, 2016.

Sourav Sarkar, Department of Physics, Indian Institute of Technology, Delhi (New Delhi). India.
Dr. Jyoti Shah, Department of Material Physics and Engineering, National Physical Laboratory, New Delhi, India.
Dr. R. K. Kotnala, Department of Material Physics and Engineering, National Physical Laboratory, New Delhi, India.
Dr. Mukesh Chander Bhatnagar, Department of Physics, Indian Institute of Technology, Delhi (New Delhi). India.

co-precipitation method. They were taken in stoichiometric ratio and were mixed together in aqueous solution using minimum amount of de-ionized water. 10M NaOH solution was used as precipitating agent. The precipitation reaction follows equation,

$Co(NO_3)_2$, $6H_2O$ + $2Fe(NO_3)_3$, $9H_2O$ + 8NaOH → $CoFe_2O_4\downarrow$ + $8NaNO_3$ + $28H_2O$

Details of the synthesis procedure can be found elsewhere [11]. The precipitate was washed several times by de-ionized water prior collection. It was dried using an infrared lamp and finally grinded into fine powder.

BTO sol was prepared in nitrogen environment using barium hydroxide and titanium n-butoxide, mixed in stoichiometric ratio in 50 ml of glacial acetic acid, heated at 90°C. Citric acid was used as chelating agent. A clear sol was produced in which already prepared CFO and CZFMO nanoparticles were dispersed so as to maintain desired weight percentage with respect to BTO. Simultaneously it was sonicated and dried at 80°C in an ultrasonicator with heating arrangement until gel formation. Before drying 2 methoxy – ethanol was added to the sol to enhance gel formation. Finally obtained gel was sintered at 800°C for four hours and was grinded into fine powder after cooling down.Structural and magnetic characterizations were performed on the powder form while dielectric and optical characterizations were done on pellets. These pellets were prepared using a hydraulic press, applying a pressure of 8 tons/cm^2. The average diameter and thickness of the pellets were 9 mm and 1.5 mm respectively. Prior characterization, these pellets were sintered at different temperatures depending on their composition. Pellets with 30% magnetostrictive phase were sintered at 1150°C, those with 40% magnetostrictive phase at 1135°C and pellets with 50% magnetostrictive phase were sintered at 1120°C. Sintering duration of all these pellets was 12 hours. While pellets of individual CFO and CZFMO were sintered at 1100°C for 10 hours, sintering temperature and duration for pellet of individual BTO were 1200°C and 4 hours respectively. This kind of variation in sintering temperature was done keeping in mind that melting point of pure BTO is more than CFO or CZFMO. So it was necessary that sintering temperature was decreased as content of ferrite in the composite increased to prevent melting and possibility of chemical reaction between the phases [6]. Also high sintering temperature ensured dense microstructure of the pellets. Finally all pellets were silver painted on both sides for electric connection. In this paper, the samples with 30% of magnetostrictive phase are abbreviated as sample A (CFO – BTO_30%) and sample B (CZFMO – BTO_30%), samples with 40% of magnetostrictive phase are abbreviated as sample C (CFO – BTO_40%) and sample D (CZFMO – BTO_40%), and samples with 50% of magnetostrictive phase are abbreviated as sample E (CFO – BTO_50%) and sample F (CZFMO – BTO_50%).

Structural characterizations were done using a Phillips X'pert PRO Thin film X-ray diffractometer (CuK_α radiation; λ = 1.5406 Å), Technai G^2 20 transmission electron microscope (HRTEM), operated at 200 kV and a scanning electron microscope (SEM), model Carl Zeiss EVO 50. I-V measurements were performed with the help of a Keithley electrometer. The Attenuated Total Reflectance (ATR) measurements were carried out using the Perkin-Elmer Fourier Transform Infrared (FTIR) spectrophotometer (model Spectrum BX-2) in the wave number range 400 to 2000 cm^{-1}.The dielectric properties were measured using HP4192A LF impedance analyzer. Hysteresis loops of the powder samples were recorded using Lakeshore 7304 Vibrating Sample Magnetometer (VSM) at room temperature. PL images were recorded at room temperature using a Perkin-Elmer PL spectrometer (model LS 55) with 266 nm laser excitation source.

III. RESULTS AND DISCUSSION

A. Structural characterization:

X-ray diffraction patterns corresponding to all the individual phases and CZFMO-BTO composites have been combined in Fig. 1(a). While these patterns from both CFO and CZFMO consist of prominent cubic spinel peaks, perovskite peaks are present in case of BTO. As for the composites, patterns primarily comprise of BTO peaks, along with some suppressed peaks of CZFMO. Lesser weight percentage of CZFMO and formation of good BTO shells in the composites are the probable reasons behind this variation in intensity of these two kind of peaks. Fig. 1(b) shows that diffraction angle corresponding to (311) peak in CZFMO shifts towards slightly smaller value than in CFO. It signifies an increase in lattice parameter of CZFMO than that of CFO. Since ionic radius of Zn (0.65 A) is larger than that of Co (0.6 A), substitution of Zn at the site of Co resulted in increase of lattice parameter. Also broadness of the spinel peaks clearly suggests formation of nano sized ferrite particles [4,12]. We have calculated the lattice parameters of the phases in all samples as well as crystallite sizes using well-known Debye-Scherrer formula and these results have been tabulated in Table 1.

HRTEM micrographs in Fig. 2 reveal core shell type particle formation in sample B. In Fig. 2(a), area with brighter contrast corresponds to BTO which encapsulates the less bright area corresponding to CZFMO. The average diameter of CZFMO is ~ 50 nm which is significantly higher than the calculated crystallite size from X-ray diffraction data. Agglomeration of ferromagnetic CZFMO nanoparticles might be the reason here. Clear interface between the two phases and lattice planes inCZFMO are prominent in Fig. 2(b). Fig. 2(c) shows an enlarged view of the interface in Fig. 2(a) which clearly reveals the planes of both phases. These planes have been identified and indexed based on the calculation of inter-planar spacing using ImageJ software. Fig. 2(d) and 2(e) present the Fast Fourier Transform (FFT) images of these planes of CZFMO and BTO respectively.

Quantitative elemental analysis suggests that no impurity other than the constituent elements were present in both individual and composite samples. EDX spectra of CFO, CZFMO, sample E and sample F in Fig. 3(a), (b), (c) and (d) respectively also show that the actual weight percentage of the two phases varies within ± 5% of the calculated value. The weight percentage and the atomic percentage of all elements in these samples from EDX analysis have been

tabulated in Table 2. They are in good agreement with our proposed composition of the samples.

I-V measurement was carried out on ferrite materials using two probe methods to find out the effect of the substitution of Zn and Mn on the resistivity of CFO. To our satisfaction, we observed that the resistivity was one order higher in the substituted composite CZFMO, as can be clearly seen in Fig. 4. Certainly it would be a promising candidate in place of CFO in multiferroic composites.

Particle formation of individual phases in all samples is evident in SEM micrographs 5(a), (b), (c), (d), and (e). Fig. 5(a) shows homogeneous distribution of CFO particles with dense microstructure. The particles are of uniform size, without any particular shape. Melting and agglomeration can be seen in case of CZFMO sample (Fig. 5(b)) along with not so dense microstructure. Sintering of the pellet at high temperature is a probable reason. The composite samples (sample B, D and F), however, do not pose these problems. Fig. 5(c), (d) and (e) clearly show existence of particles of both phases with compact packing. Particles with brighter contrast and better crystallinity correspond to BTO phase while those with less bright contrast and little agglomeration are of CZFMO.

ATR-FTIR spectra in Fig. 6(a) include response of sample A, C and E along with pure CFO and BTO while Fig. 6(b) sum up the behaviour of sample B, D and F along with their constituents phases. The most prominent band for pure CFO at 584 cm^{-1} in Fig. 6(a) can be attributed to the stretching vibration of the tetrahedral groups (Fe^{3+}-O^{2-}). Vibration mode for octahedral groups (Fe^{3+}-$O^{2-}$and Co^{2+}-O^{2-}) generally appear below 400 cm^{-1} which could not be recorded due to the instrument's limitation [13–15]. Some Fe-Co alloy might be present in CFO which are responsible for the band at 864 cm^{-1}. For BTO, some residual organic groups might remain from synthesis which could be the reason for the band at 1508 cm^{-1}[16–19]. In composites also, only these bands are present which rules out the possibility of other impurity phases. Less prominence of both bands (at 584 $cm^{-1}$and 864 cm^{-1}) in the composites can be an indirect proof of good BTO shell formation around CFO core. In all the samples, a band appears at 1444 cm^{-1} which might be due to the presence of moisture from ambience. In Fig. 6(b), the tetrahedral band in CZFMO shifts towards higher wave number (588 cm^{-1}). It essentially proves that Mn ions have substituted part of Fe ions at tetrahedral sites in CZFMO, because the ionic radius of Mn cation (0.58 A) is smaller than that of Fe cation (0.64 A). The presence of other bands have already been explained.

B. Dielectric characterization

Fig.7(a) and (b) depicts the frequency variation of dielectric constant (ε) and dielectric loss (tanδ) respectively of all CZFMO-BTO composites at room temperature. At a certain frequency, ε is maximum for sample A and decreases as concentration of CZFMO increases. This is due to the difference in resistivity of CZFMO and BTO. This is why tanδ is minimum for sample A and dielectric loss increases with increasing concentration of CZFMO. Now the nature of variation of ε and tanδ with frequency is same for all the samples. Both have higher value at lower frequency and gradually decrease with increase in frequency. This phenomena can be explained by Maxwell-Wagner interfacial polarization theory [6,20,21]. According to this, space charge accumulates at the interface of multiphase composites with different dielectric structures and resistivity values. These space charges align themselves along the direction of the applied alternating electric field. This kind of buildup requires finite time and as the frequency increases it becomes difficult for the space charges to catch up with the alternating field. As a result, both ε and tanδ decreases.

Interesting features came to the fore when we investigated the temperature variation of ε and tanδ of CZFMO-BTO composites at different frequencies. Fig. 8(a), (b), (c) and (d) record the variation of ε at 1 kHz, 10 kHz, 100 kHz and 1 MHz respectively. Same variation for CFO-BTO composites at these frequencies have been shown in the inset of these figures. Since dielectric property of composites depends on the contribution from all the phases involved, we have to take into account the effect of BTO and CZFMO separately. The first thing we notice is that at all frequencies ε increases with increasing temperature, shows one anomaly above 200°C, again increases and finally gives a glimpse of a second anomaly around 500°C. The first anomaly can be attributed to the ferroelectric to paraelectric transition of BTO which occurs in the temperature range 120°C-150°C in pure BTO. The shift in Curie temperature (T_C) in the composites is due to the presence of CZFMO in BTO matrix which reduces the c/a ratio of BTO. As a consequence, the anomaly moves towards higher temperature with increase in mole percentage of CZFMO. Another characteristics of this anomaly is that it shifts towards higher temperature with increase in frequency which is a typical feature of relaxor type ferroelectrics. The high temperature variation and second anomaly can be explained by the contribution of CZFMO. The primary source of dielectric behaviour of ferrites are the hopping electrons which come from the electron exchanges $Fe^{2+} \Leftrightarrow Fe^{3+} + e^{-1}$, and $Mn^{2+} \Leftrightarrow Mn^{3+} + e^{-1}$along with hopping holes from the exchange $Co^{3+} \Leftrightarrow Co^{2+}$ in case of CZFMO. This mechanism dominates at high temperature and contributes significantly towards the increase of dielectric response of the composites. Butat sufficiently high temperature the thermal energy starts to catch up with the potential barrier related to domain wall movement and reaches a maximum around the magnetic Curie temperature (T'_C ~ 520°C for CFO) [22].Above T'_C, magnetic domains disappear as the ferrites attain paramagnetic state and consequently dielectric response diminishes [21,23] as can be prominently seen for sample A in the inset of Fig. 8(d). Sample B shows a glimpse of this nature in Fig. 8(c) which helps us to draw the conclusion that substitution of Zn and Mn in CFO increases T'_C. Fig. 9(a), (b), (c) and (d) record the variation of tanδ at 1 kHz, 10 kHz, 100 kHz and 1 MHz respectively. Same variation for CFO-BTO composites at these frequencies have been shown in the inset of these figures. Peaks are present in the variation of all samples which tend to shift towards higher temperature at had frequency. This feature is again attributed to the hopping conduction in ferrites.

C. Magnetic characterization

Magnetic characterization was performed on all the composites as well as individual ferrites at room temperature. M-H curves in Fig. 10(a) and (b) are corresponding to CFO-BTO and CZFMO-BTO composites respectively. Hysteresis loops of regarding individual ferrites can be seen in the inset of these figures. As expected, these loops are ferromagnetic in nature where saturation magnetization (M_S) increases linearly with increase of ferrite component in the composites and coercive field (H_C) increases when a non-magnetic shell of BTO is put around the ferromagnetic core. Table 1 contains the M_S, M_R and H_C values of all samples. We notice that the M_S value corresponding to CFO here is way below than its bulk counterpart (i.e. M_S for bulk CFO ~ 65 emu/g). This can be attributed to the formation of magnetic nanoparticles with very small crystallite sizes. They give rise to various contributing factors such as electron spin canting at the surface, formation of dead surface layers etc. which combine to bring down the saturation magnetization value [10]. Presence of diamagnetic BTO shell is responsible for the decrease of H_C valuein the composites as it makes movement of magnetic domains and rotation of magnetic moment harder. Fig. 10(b) reveals that substitution of Zn and Mn in CFO results in decrease of M_S value which can be explained on the basis of Neel's two sublattice model of ferrimagnetism [24]. Since magnetization of ferrimagnetic spinels depends on the exchange interaction between the magnetic moments of tetrahedral A sublattice and octahedral B sublattice, substitution of non-magnetic Zn^{2+} ions at A site effectively influences the interaction, hence lowering M_S value ultimately. Remnant magnetization (M_R) value also decreases substantially in CZFMO-BTO composites as can be seen in Table 1. By controlling the amount of substitution, we can tailor the magnetic properties of CFO efficiently [6,24].

D. Optical characterization

PL spectrum of pure CFO in Fig. 11(a) give an insight about the energy band gap of the ferrite and Fig. 11(b) reveals the effect of substitution of Zn and Mn in that spectrum. PL spectra of pure BTOand CZFMO-BTO composites have also been recorded in Fig. 11(b).Principalemission peak corresponding to pure CFO is centered at 370 nm and results from presence of quantum confinement as corresponding energy is of the order of the band gap of ferrite materials (~3 eV)[10,25]. In CZFMO this peak shifts towards slightly higher wavelength (~372 nm) and it is relatively broader. Substituted Zn^{2+} and Mn^{2+}ionsmight have worked as electron traps and gave rise to intermediate energy levels. Emission peak corresponding to pure BTO is centered at 361 nm as can be seen in Fig. 11(b). Thiscan be attributed to the presence of O-Ti-O network which is inevitably and intermediately formed during the formation of oxygen octahedra (TiO_6) enclosing Ti^{4+} ion[26]. Now for the composites, a doublet structure in the emission peak was expected. Instead we get intermediate and broad emission peaks for sample B and sample D. But sample F with highest weight percentage of CZFMO peaks at higher wavelength than pure CZFMO, though retaining the broadness. This can be explained on the basis of comparison between the excitation wavelength (266 nm) and dimension of the particles in the composites. Since average diameter of the particles were less than 50 nm with a prominent core shell like structure, as can be seen in HRTEM micrographs, an excitation wavelength of 266 nm could probably not penetrate a shell of 15 nm. Hence, the doublet structure is missing.Another peak appeared around 469 nm (2.66 eV) for all the samples except pure BTO which can be attributed to the presence of singly charged oxygen vacancies. Since doubly ionized oxygen vacancies are most common form of defects, present in perovskites and spinels, they tend to neutralize while treated in high temperature post synthesis. It may so happen during this process that some of the doubly ionized vacancies undergo incomplete neutralization and become singly charged which are responsible for this peak [27,28]. For pure BTO this peak can be found at slightly lower wavelength (459 nm) which might be due to some deviation in preparation conditions.

IV. CONCLUSION

In short, we have synthesized Zn and Mn substituted $CoFe_2O_4$ and used it as core material in our proposed core-shell type composite. The substituted material, abbreviated here as CZFMO, retains the structural property of CFO. Increase in lattice parameter after substitution can be attributed to the larger ionic radius of Zn than Co. HRTEM micrographs show core-shell type structure with presence of planes of both CZFMO and BTO at the interface. Both ATR-FTIR and PL spectra confirm our proposed substitution in CFO. Variation of dielectric parameters with temperature as well as frequency has been explained on the basis of hopping conduction in ferrites and Maxwell Wagner relaxation of charges at the interface. Also it indirectly suggests increase in magnetic Curie temperature of the substituted composites. Magnetic hysteresis loops show considerable decrease in coercivity as well as retentivity after substitution and show traits of superparamagnetism. Most importantly, resistivity of CZFMO has been found to be one order higher than CFO which makes it a suitable replacement for CFO in multiferroic core-shell type composites for achieving larger magnetoelectric voltage response.

ACKNOWLEDGEMENTS

Authors would like to acknowledge Nano Science Unit of NSTI, DST, IIT Delhi for acquiring HRTEM micrographs. They would like to thank Prof. Ratnamala Chatterjee in IIT Delhi for the dielectric measurements. Optical characterization was carried out under Nanophotonic material high-impact research scheme of IIT Delhi. One of the authors (SS) acknowledges CSIR, India for providing fellowship.

REFERENCES

1. J. Ryu, S. Priya, K. Uchino, H.E. Kim, Magnetoelectric Effect in Composites of Magnetostrictive and Piezoelectric Materials,J. Electroceram, (2002) 107–119. doi:10.1023/A.
2. G.V. Duong, R. Groessinger, R.S. Turtelli, Magnetoelectric properties of CoFe2O4 –BaTiO3

magnetoelectric composites, J. Magn. Magn. Mater. 316 (2007) 624–627. doi:10.1016/j.jmmm.2007.03.142.
3. N.A. Spaldin, M. Fiebig, The Renaissance of Magnetoelectric Multiferroics, Science 309 (2005) 391–392. doi:10.1126/science.1113357.
4. Corral-Flores, D. Bueno-Baques, R.F. Ziolo, Synthesis and characterization of novel CoFe2O4-BaTiO3 multiferroic core-shell-type nanostructures, Acta Mater. 58 (2010) 764–769. doi:10.1016/j.actamat.2009.09.054.
5. G. V. Duong, R. Groessinger, M. Schoenhart, D. Bueno-Basques, The lock-in technique for studying magnetoelectric effect, J. Magn. Magn. Mater. 316 (2007) 390–393. doi:10.1016/j.jmmm.2007.03.185.
6. Gupta, R. Chatterjee, Dielectric and magnetoelectric properties of BaTiO3-Co0.6Zn0.4Fe1.7Mn0.3O4 composite, J. Eur. Ceram. Soc. 33 (2013) 1017–1022. doi:10.1016/j.jeurceramsoc.2012.11.003.
7. P. Zhu, Q. Zheng, R. Sun, W. Zhang, J. Gao, C. Wong, Dielectric and magnetic properties of BaTiO3/Ni0.5Zn0.5Fe2O4 composite ceramics synthesized by a co-precipitation process, J. Alloys Compd. 614 (2014) 289–296. doi:10.1016/j.jallcom.2014.06.065.
8. G.S. Shahane, A. Kumar, M. Arora, R.P. Pant, K. Lal, Synthesis and characterization of Ni-Zn ferrite nanoparticles, J. Magn. Magn. Mater. 322 (2010) 1015–1019. doi:10.1016/j.jmmm.2009.12.006.
9. K. Raidongia, A. Nag, A. Sundaresan, C.N.R. Rao, Multiferroic and magnetoelectric properties of core-shell CoFe2O4 @ BaTiO3 nanocomposites, Appl. Phys. Lett. 97 (2010) 2010–2012. doi:10.1063/1.3478231.
10. R.K. Singh, A. Narayan, K. Prasad, R.S. Yadav, A.C. Pandey, A.K. Singh, L. Verma, R.K. Verma, Thermal, structural, magnetic and photoluminescence studies on cobalt ferrite nanoparticles obtained by citrate precursor method, J. Therm. Anal. Calorim. 110 (2012) 573–580. doi:10.1007/s10973-012-2728-1.
11. S. Sarkar, M.C. Bhatnagar, Effect of Mn substitution on acetone and ammonia sensing in CoFe2O4nanoparticles, 2nd Int. Symp. Phys. Technol. Sensors, IEEE, 2015: pp. 253–256. doi:10.1109/ISPTS.2015.7220123.
12. G. Vaidyanathan, S. Sendhilnathan, R. Arulmurugan, Structural and magnetic properties of Co1-xZnxFe2O4 nanoparticles by co-precipitation method, J. Magn. Magn. Mater. 313 (2007) 293–299. doi:10.1016/j.jmmm.2007.01.010.
13. L. Zhao, H. Zhang, Y. Xing, S. Song, S. Yu, W. Shi, X. Guo, J. Yang, Y. Lei, F. Cao, Studies on the magnetism of cobalt ferrite nanocrystals synthesized by hydrothermal method, J. Solid State Chem. 181 (2008) 245–252. doi:10.1016/j.jssc.2007.10.034.
14. S. Singhal, S. Bhukal, J. Singh, K. Chandra, S. Bansal, Optical, X-ray diffraction, and magnetic properties of the cobalt-substituted nickel chromium ferrites (CrCox Ni1-xFeO4, x = 0, 0.2, 0.4, 0.6, 0.8, 1.0) synthesized using sol-gel autocombustion method, J. Nanotechnol. 2011 (2011) 2–7. doi:10.1155/2011/930243.
15. R.M. Mohamed, M.M. Rashad, F.A. Haraz, W. Sigmund, Structure and magnetic properties of nanocrystalline cobalt ferrite powders synthesized using organic acid precursor method, J. Magn. Magn. Mater. 322 (2010) 2058–2064. doi:10.1016/j.jmmm.2010.01.034.
16. H. Deligöz, A. Baykal, M.S. Toprak, E.E. Tanriverdi, Z. Durmus, H. Sözeri, Synthesis, structural, magnetic and electrical properties of Co1-xZnxFe2O4 (x = 0.0, 0.2) nanoparticles, Mater. Res. Bull. 48 (2013) 646–654. doi:10.1016/j.materresbull.2012.11.032.
17. S.J. Chang, W.S. Liao, C.J. Ciou, J.T. Lee, C.C. Li, An efficient approach to derive hydroxyl groups on the surface of barium titanate nanoparticles to improve its chemical modification ability, J. Colloid Interface Sci. 329 (2009) 300–305. doi:10.1016/j.jcis.2008.10.011.
18. U.-Y. Hwang, H.-S. Park, K.-K. Koo, Behavior of Barium Acetate and Titanium Isopropoxide during the Formation of Crystalline Barium Titanate, Ind. Eng. Chem. Res. 43 (2004) 728–734. doi:10.1021/ie030276q.
19. H. Reverón, C. Aymonier, A. Loppinet-Serani, C. Elissalde, M. Maglione, F. Cansell, Single-step synthesis of well-crystallized and pure barium titanate nanoparticles in supercritical fluids, Nanotechnology. 16 (2005) 1137–1143. doi:10.1088/0957-4484/16/8/026.
20. Y. Wang, Y. Wang, W. Rao, M. Wang, G. Li, Y. Li, J. Gao, W. Zhou, J. Yu, Dielectric, ferromagnetic and ferroelectric properties of the (1 − x)Ba0.8Sr0.2TiO3–xCoFe2O4 multiferroic particulate ceramic composites, J. Mater. Sci. Mater. Electron. 23 (2012) 1064–1071. doi:10.1007/s10854-011-0548-x.
21. I.H. Gul, A. Maqsood, M. Naeem, M.N. Ashiq, Optical, magnetic and electrical investigation of cobalt ferrite nanoparticles synthesized by co-precipitation route, J. Alloys Compd. 507 (2010) 201–206. doi:10.1016/j.jallcom.2010.07.155.
22. Gupta, R. Chatterjee, Study of dielectric and magnetic properties of PbZr0.52Ti0.48O3-Mn0.3Co0.6Zn0.4Fe1.7O4 composite, J. Magn. Magn. Mater. 322 (2010) 1020–1025. doi:10.1016/j.jmmm.2009.12.007.
23. V Shvartsman, F. Alawneh, P. Borisov, D. Kozodaev, D.C. Lupascu, Converse magnetoelectric effect in CoFe2O4 –BaTiO3 composites with a core–shell structure, Smart Mater. Struct. 20 (2011) 075006. doi:10.1088/0964-1726/20/7/075006.
24. S. Singhal, T. Namgyal, S. Bansal, K. Chandra, Effect of Zn Substitution on the Magnetic Properties of Cobalt Ferrite Nano Particles Prepared Via Sol-Gel Route, J. Electromagn. Anal. Appl. 02 (2010) 376–381. doi:10.4236/jemaa.2010.26049.
25. Y. Fu, H. Chen, X. Sun, X. Wang, Combination of cobalt ferrite and graphene: High-performance and recyclable visible-light photocatalysis, Appl. Catal. B Environ. 111-112 (2012) 280–287. doi:10.1016/j.apcatb.2011.10.009.
26. N. V. Dang, T.L. Phan, T.D. Thanh, V.D. Lam, L. V. Hong, Structural phase separation and optical and magnetic properties of BaTi1-xMnxO3 multiferroics, J. Appl. Phys. 111 (2012). doi:10.1063/1.4725195.
27. K. Vanheusden, W.L. Warren, C.H. Seager, D.R. Tallant, J.A. Voigt, B.E. Gnade, Mechanisms behind green photoluminescence in ZnO phosphor powders, J. Appl. Phys. 79 (1996) 7983. doi:10.1063/1.362349.
28. Warren, W.L., Vanheusden, K., Dimos, D., Pike, G.E. and Tuttle, B.A., 1996. Oxygen vacancy motion in perovskite oxides. J. Am. Ceram. Soc. 79(2), pp.536-538.

FIGURE CAPTIONS

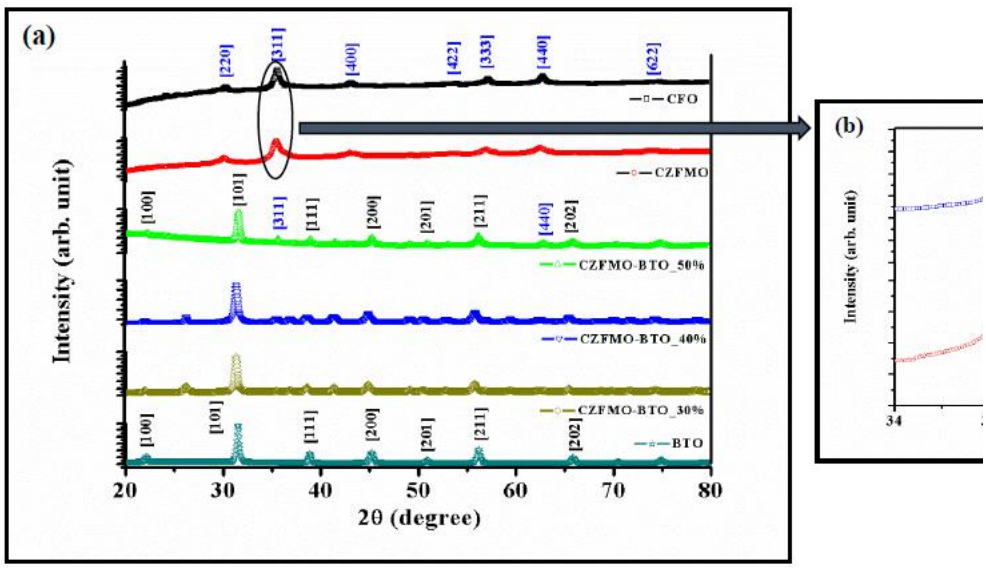

Fig. 1. (a) XRD patterns of CFO, CZFMO, sample A, sample B, sample C, and BTO, and (b) enlarged view of the (311) peak shift in CZFMO, compared to CFO

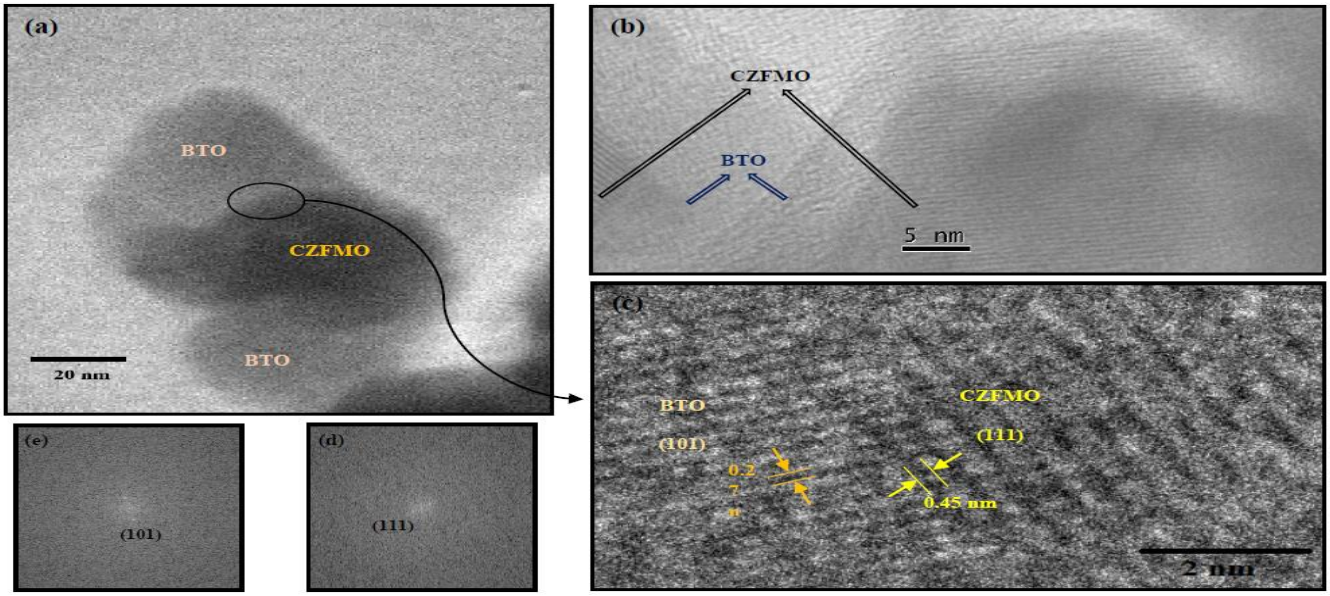

Fig. 2. HRTEM micrograph corresponding to sample B showing (a) core-shell type structure, (b) clear interface and lattice planes corresponding to CZFMO, (c) magnified view of the interface in fig. 2 (a) showing (110), and (101) planes corresponding to CZFMO, and BTO respectively, (d), and (e) FFT images corresponding to CZFMO, and BTO planes respectively

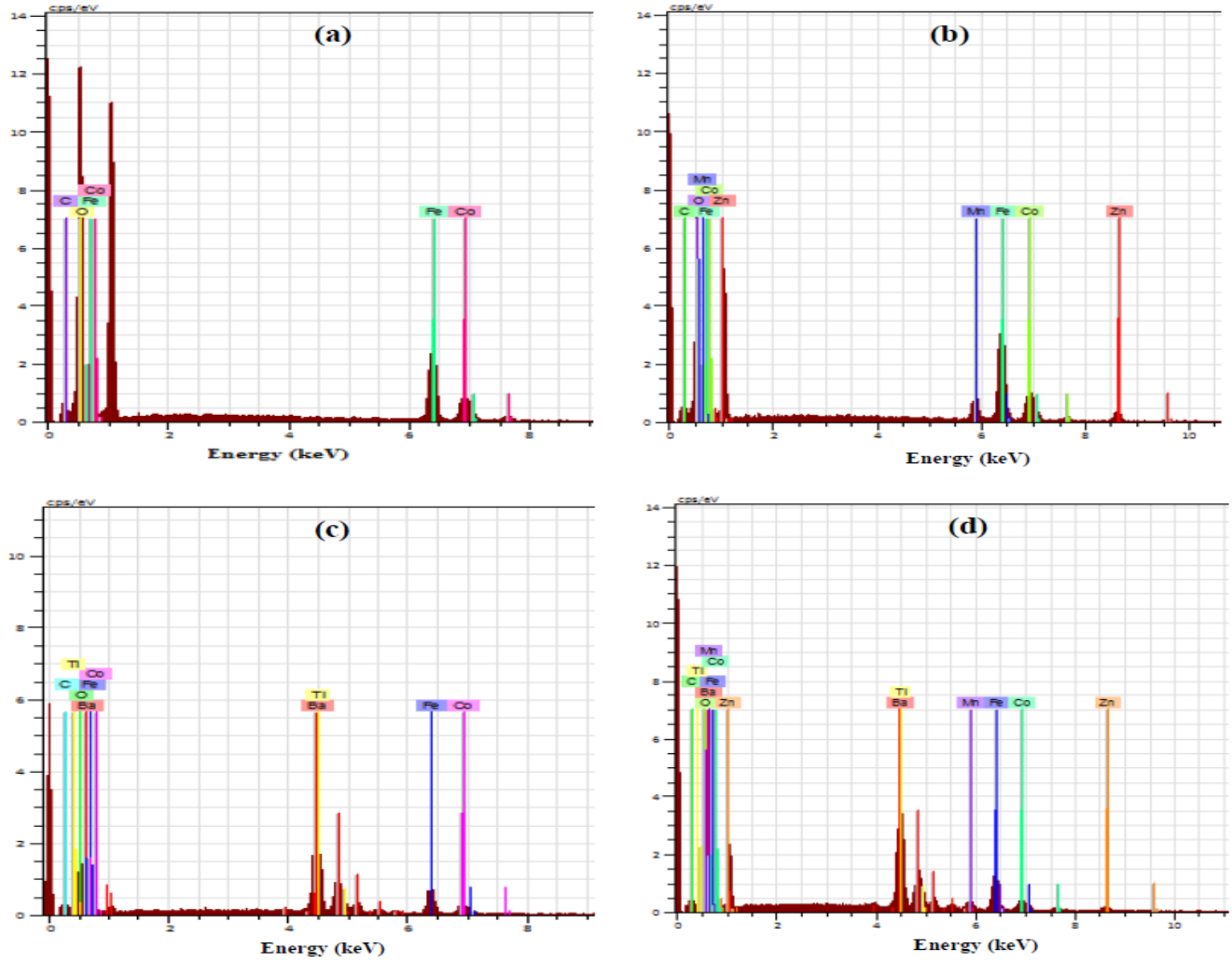

Fig. 3. EDX spectra of (a) CFO, (b) CZFMO, (c) sample E, and (d) sample F

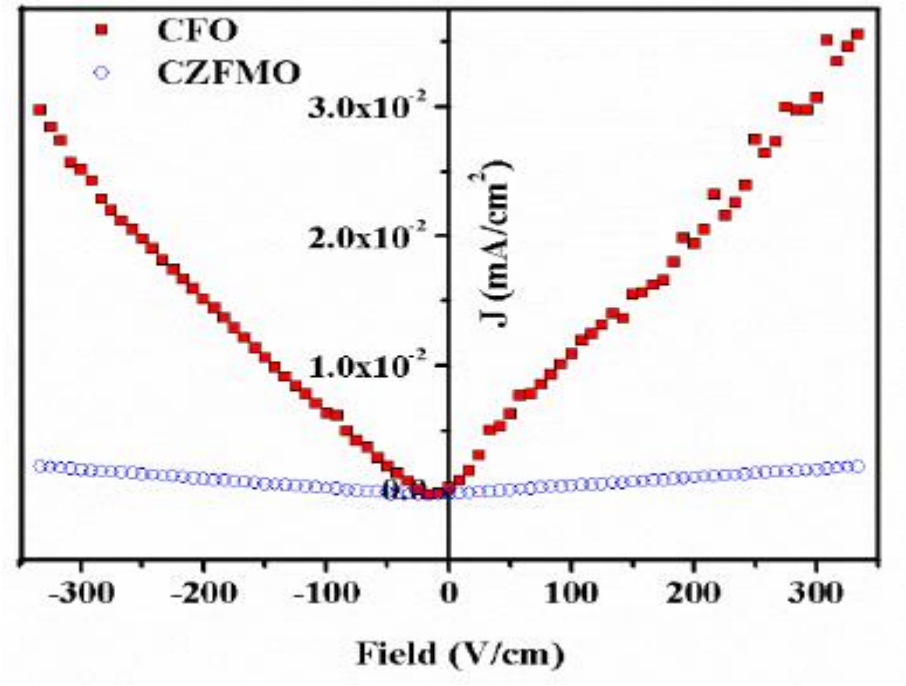

Fig. 4. Current density (J) vs. applied field plot for CFO and CZFMO

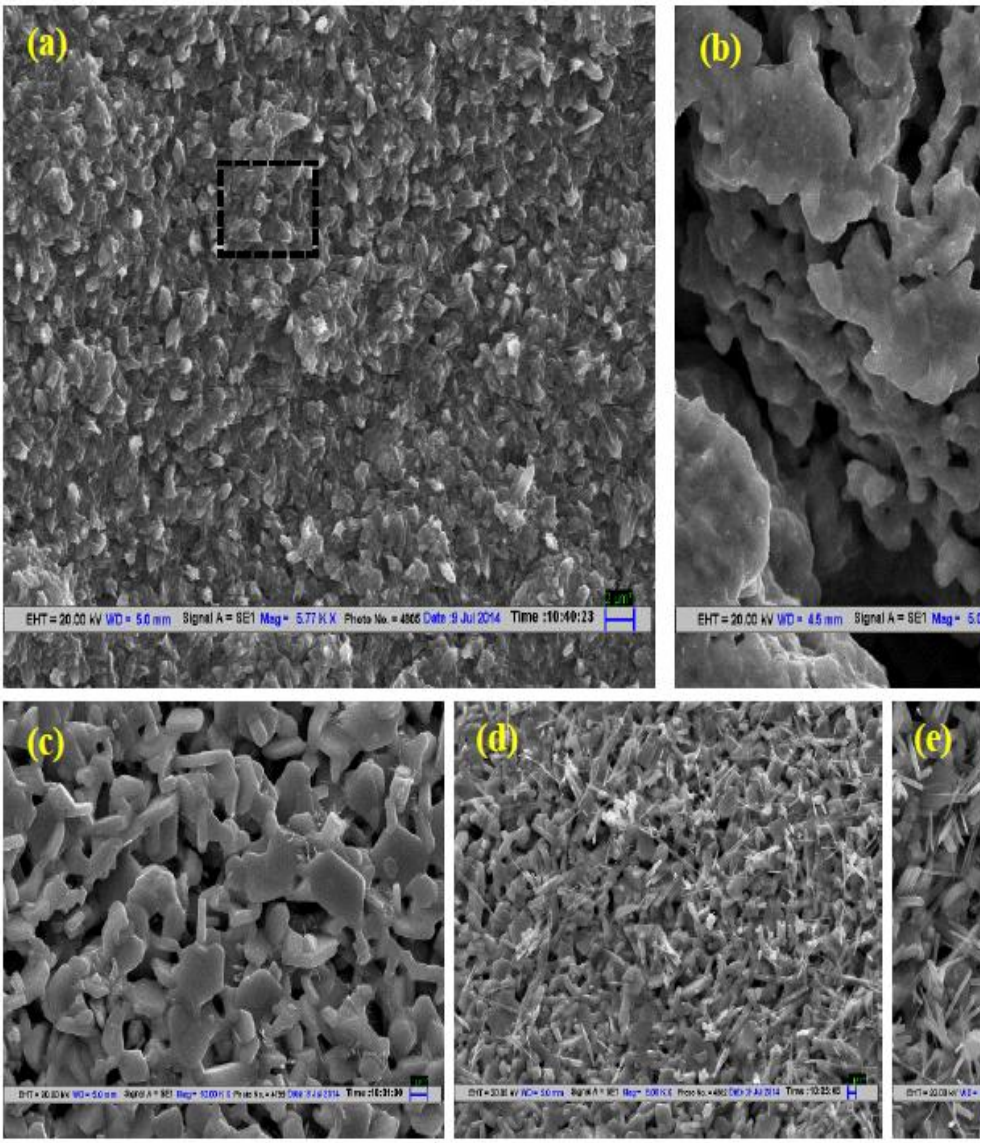

Fig. 5. Scanning Electron Micrographs for (a) CFO, (b) CZFMO, (c) sample B, (d) sample D, and (e) sample F in pellet form (selected areas from Fig. 5 (a), (b), and (e) provide EDX spectra, shown in Fig. 3)

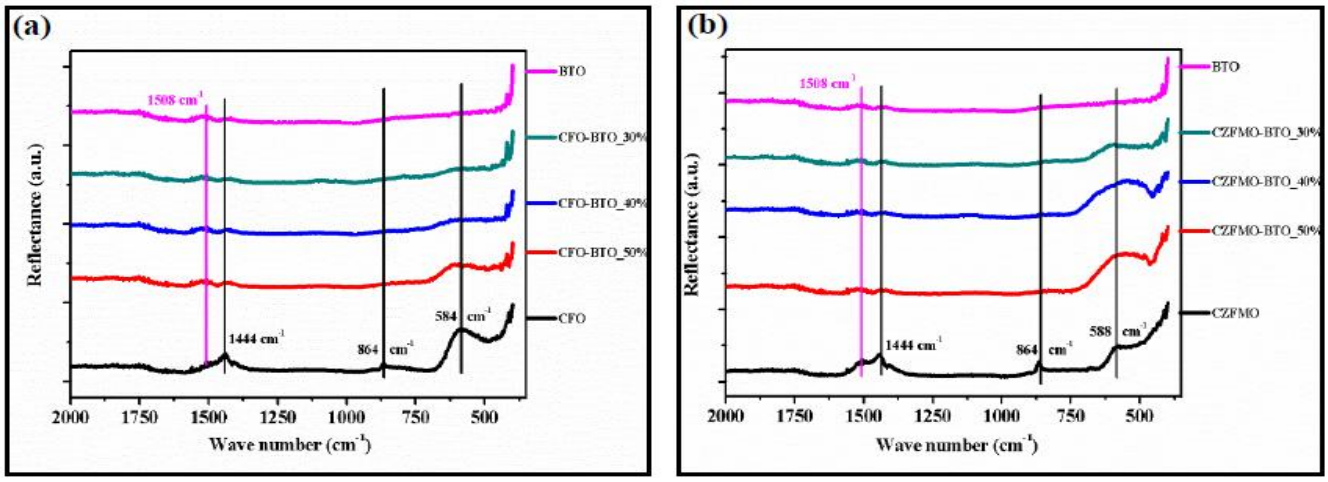

Fig. 6. ATR-FTIR spectra corresponding to (a) CFO, BTO, and CFO-BTO composites, and (b) CZFMO, BTO, and CZFMO-BTO composites

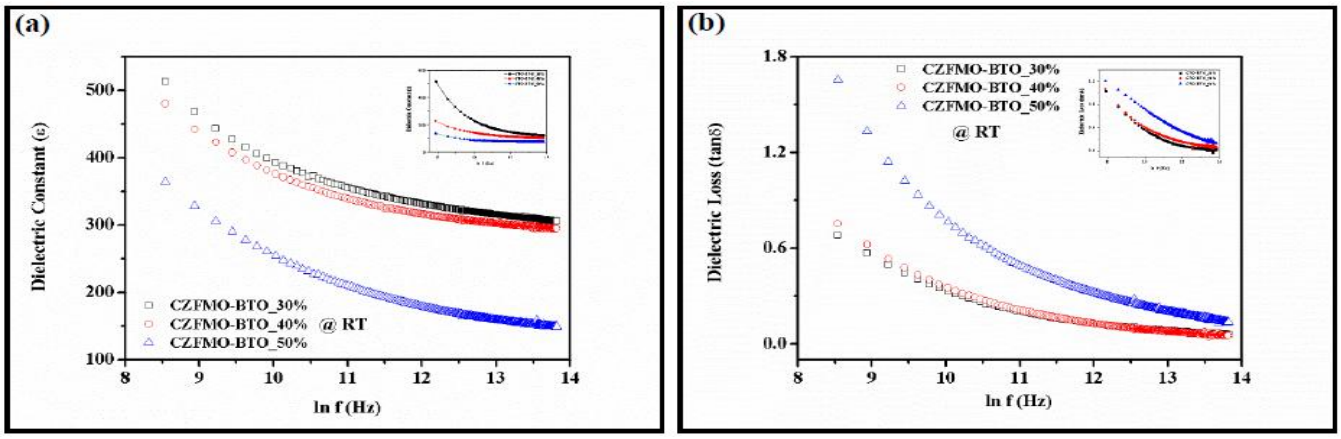

Fig. 7. Variation of (a) dielectric constant (ε), and (b) dielectric loss (tanδ) with frequency (Hz) for CZFMO-BTO composites at room temperature (27°C) (inset shows same plots for CFO-BTO composites)

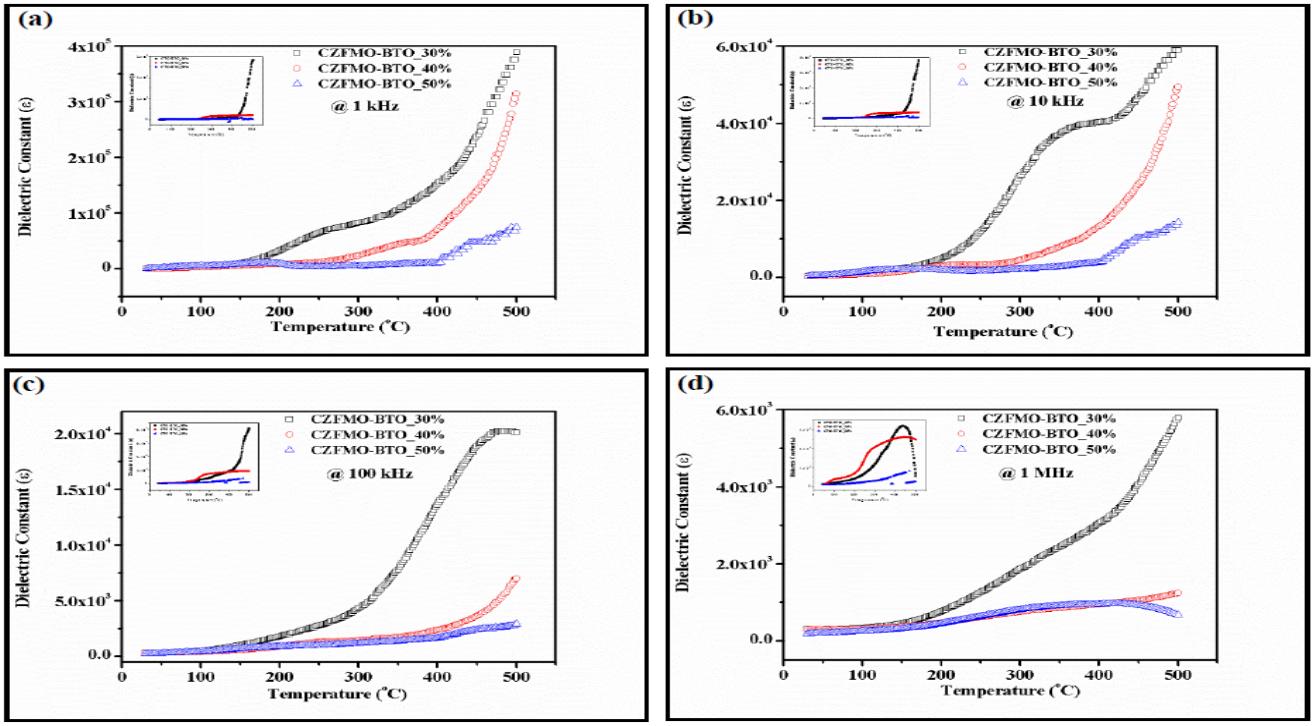

Fig. 8. Variation of dielectric constant (ε) with temperature (T) for CZFMO-BTO composites at (a) 1 KHz, (b) 10 KHz, (c) 100 KHz, and (d) 1 MHz (inset shows same plots for CFO-BTO composites)

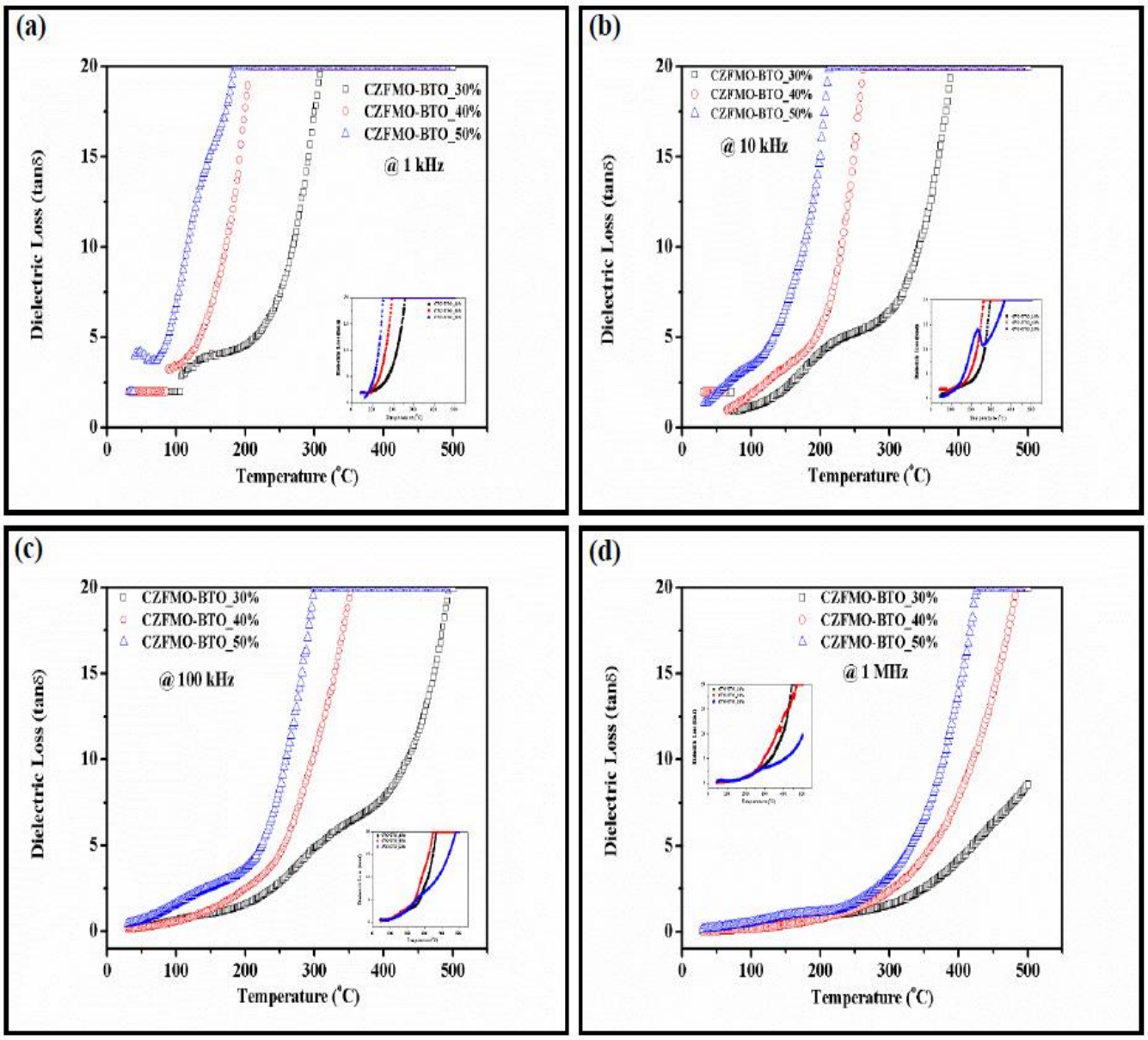

Fig. 9. Variation of dielectric loss (tanδ) with temperature (T) for CZFMO-BTO composites at (a) 1 KHz, (b) 10 KHz, (c) 100 KHz, and (d) 1 MHz (inset shows same plots for CFO-BTO composites)

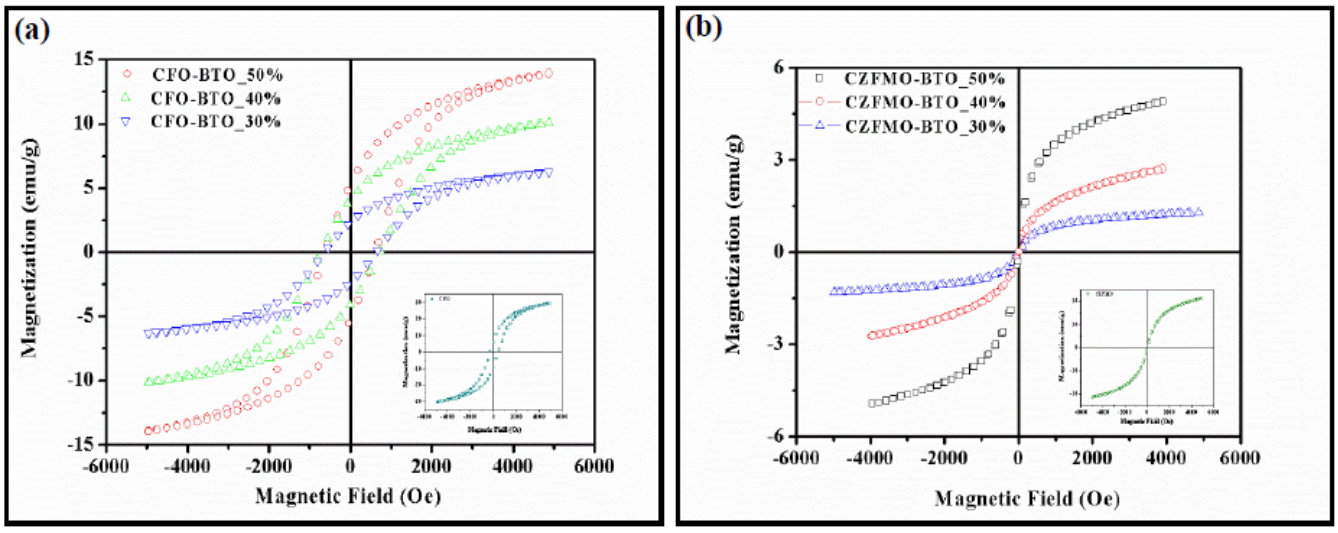

Fig. 10. Magnetization (M) vs. magnetic field (H) plot for (a) CFO-BTO composites (M-H loop for CFO is shown in inset), and (b) CZFMO-BTO composites (M-H loop for CZFMO is shown in inset)

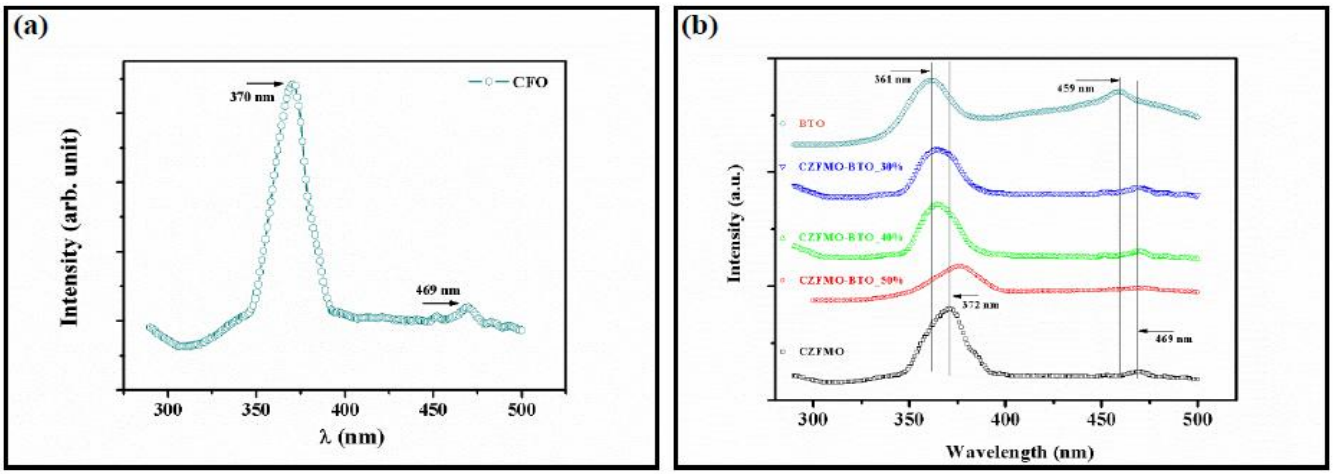

Fig. 11. Photoluminescence spectra for (a) CFO, and (b) CZFMO, BTO, CZFMO-BTO composites using a laser excitation source of 266 nm

TABLE CAPTION

Table 1. Average crystallite sizes, lattice parameters, saturation magnetization, remnant magnetization, and coercively of the samples

Sample	Average Crystallite sizes (nm)		Lattice parameters (Å)			M_S	M_R	H_C
	$CoFe_2O_4$	$BaTiO_3$	$CoFe_2O_4$		$BaTiO_3$	(emu/g)	(emu/g)	(Oe)
	a	*a*	*a*	*c*				
CFO	16		8.370			29.9	5.9	342.1
CZFMO	13		8.393			21.3	0.3	20.5
A	17	17	8.352	4.0147	4.015	6.3	2.1	654.1
B	23	25	8.396	4.039	4.0286	1.3	0.05	35.8
C	29	24	8.385	4.0288	4.022	10.1	3.6	711.9
D	18	23	8.396	4.0359	4.0286	2.7	0.03	20.9
E	15	25	8.395	4.0204	4.0215	13.9	4.9	559.2
F	28	21	8.397	4.0045	4.0136	4.9	0.06	20.6
BTO		17		3.9679	4.0352			

Table 2. Quantitative elemental analysis using EDX spectra for CFO, CZFMO, CFO-BTO_50%, and CZFMO-BTO_50%

Fig.	Element	Weight%	Atomic%
3.a	O K	37.72	54.88
	Co K	18.55	6.33
	Fe K	30.86	12.86
3.b	O K	35.78	52.79
	Co K	13.24	5.30
	Fe K	26.57	11.23
	Zn K	7.12	2.57
	Mn K	3.82	1.64
3.c	O K	38.70	60.66
	Ba L	31.83	5.81
	Ti K	10.53	5.32
	Co K	4.65	1.98
	Fe K	7.85	3.72
3.d	O K	42.46	65.57
	Ba L	27.82	5.01
	Ti K	9.53	4.38
	Co K	3.14	1.32
	Fe K	7.83	3.47
	Zn K	2.96	1.12
	Mn K	1.23	0.55

AUTHOR PROFILE

Sourav Sarkar, received his Bachelor of Science (Hons) degree in Physics from Calcutta University, India and Master of Science (M.Sc) degree in Physics from Indian Institute of Technology, Delhi (IIT Delhi), India in 2008 and 2010 respectively. He was joint recipient of Jagat Ram Chopra Award for Best Thesis by a Master's student at IIT Delhi in 2010. He is currently pursuing his Ph.D from Physics Department, IIT Delhi. His broad area of research includes Multiferroic Composite materials, and Ferrite based Sensors.

Dr. Jyoti Shah, is currently working as DST-Women Scientist at CSIR-National Physical Laboratory, India. She has authored more than 75 journal papers. An expert in numerous characterization techniques, her research interest includes Material Science, Spectroscopy, Thin Films, Nanotechnology and Nanomaterials, and many more.

Dr. R. K. Kotnala, is a Chief Scientist (Scientist for last 33 years in NPL, New Delhi) & Head of Materials Physics & Engineering Division, National Physical Laboratory, New Delhi. He obtained Ph.D in Solar Cell from IIT Delhi in 1982. He is an Associate Editor for last two years in Journal of Applied Physics, AIP, NewYork, USA. He has published 305 research papers in prestigious international journals, has 681 citations only in last 10 months, has 6 US/ Indian patents, 9 industrial consultancies & support to 112 industries. He has given more than 310 invited talks, and has authored 4 books. His areas of specialization are Magnetic Measurements standards, Nano Magnetic Material, Superconductivity, Multiferroics, CMR Materials, DMS, Spintronic Device Physics, Solar Cell, Humidity Sensor, and Hydroelectric Cell.

Dr. M.C. Bhatnagar is an Associate Professor at the department of Physics, IIT Delhi. He received his M.Sc (Physics) and M.Tech (Microwave Engineering) from University of Delhi and PhD in the field of solar cells from IIT Delhi. His current area of research includes development of humidity and gas sensors, ferrite based sensors, associated electronics and instrumentation, and gas sensitivity improvement by ion beam irradiation.